Temperature-Responsive Nanoporous Membranes from Self-Assembly of Poly(*N*-isopropylacrylamide) Hairy Nanoparticles

Yulia Eygeris,† Qiaoyi Wang,† Marion Görke, Michael Grünwald, and Ilya Zharov**

Department of Chemistry, University of Utah, 315 South 1400 East, Salt Lake City, UT, 84112

ABSTRACT: Nanoporous membranes play a critical role in numerous separations on laboratory and industrial scales, ranging from water treatment to biotechnology. However, few strategies exist that allow for the preparation of mechanically robust nanoporous membranes whose separation properties can be easily tuned. Here, we introduce a new family of tunable nanoporous membranes based on nanoparticles decorated with temperature responsive polymer brushes. We prepared mechanically robust membranes from hairy nanoparticles (HNPs) carrying PNIPAM polymer brushes. We assembled the HNPs into thin films through pressure-driven deposition of nanoparticle suspensions and measured the permeability and filtration cutoff of these membranes at different temperatures. The membrane pore diameter at room temperature varied between 10 and 30 nm depending on the polymer length. The water permeability of these membranes could be controlled by temperature, with the effective pore diameter increasing by a factor of 3-6 (up to 100 nm) when the temperature was increased to 60 °C. The size selectivity of these membranes in the filtration of nanoparticles could also be attenuated by temperature. Molecular dynamics computer simulations of a coarse-grained HNP model show temperature-sensitive pores sizes are consistent with our experimental results and reveal the polymer configurations responsible for the observed filtration membrane permeability. We expect that these membranes will be useful for separations and in the preparation of responsive microfluidic devices.

KEYWORDS: *nanopore, membrane, permeability, polymer brush, nanoparticle*

Introduction

Nanoporous membranes are widely used in separations because their operation is relatively simple and they are efficient in terms of energy, space, and materials.[1] Due to these advantages, nanoporous membranes find applications on industrial scale in water and wastewater treatments,[1] biotechnology,[2] and catalysis,[3] where they are used to filter suspended solids, bacteria, viruses, and ions.[4] Apart from separations, nanoporous membranes also find application in biosensing[5] and drug release.[6]

The majority of industrial separations by nanoporous membranes are based on size exclusion by nanopores of fixed size. In some cases, filtration is aided by electrostatic or non-covalent interactions due to surface modification of the nanopores. Designing nanoporous membranes whose pore size can be controlled using external stimuli such as pH,[7] light,[8] and electricity[9] can further enhance the properties of these materials. Such responsive membranes possess controlled permeability and higher selectivity, and are less susceptible to fouling.[10] They also lend themselves naturally to applications in sensing and drug release.

Common materials used to prepare nanoporous membranes include polymers,[11-13] ceramics[14,15] and zeolites.[16] To prepare responsive nanoporous membranes, two general approaches are commonly utilized. Responsive polymeric membranes are prepared using phase separation[17] or self-assembly[18] of the corresponding responsive polymers or co-polymers. Hybrid membranes are prepared from nanoporous materials by decorating them with responsive polymers either by grafting onto the plasma-activated nanopore surface,[19] or by surface-initiated polymerization.[20-22] In the past, we reported several responsive membranes produced using silica colloidal crystals as inorganic nanoporous support and polymer brushes responsive to pH, temperature and light.[23,24]

More recently, we developed a different approach to creating nanoporous membranes: self-assembly of polymer-modified ("hairy") silica nanoparticles (HNPs) into nanoporous films and free-standing membranes. In this approach, polymer brushes attached to the nanoparticle surface act as "molecular glue" to link the nanoparticles. When the polymer chains are not too long, mechanically robust nanoporous membranes are formed. This approach provides several advantages compared to conventional methods of membrane fabrications. Because the size of the silica nanoparticles and the length of the polymer brush can be varied over a wide range, the pore size in the corresponding

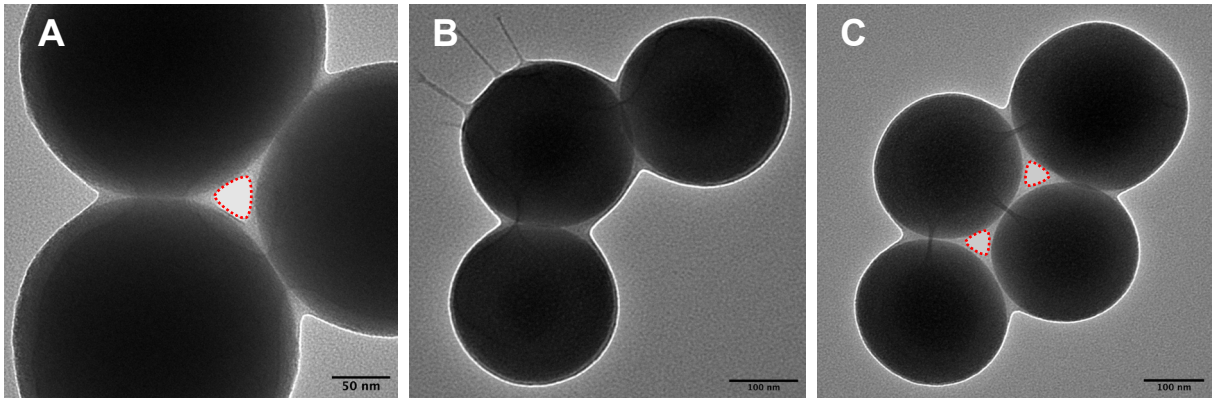

Figure 1. *TEM image of PNIPAM HNPs with different degrees of polymerization of polymer brushes: DP 80 (A), DP 250 (B), DP 450 (C). Note the difference in polymer density in the pore between triplets of HNPs for DP 80 (pore region is void of polymer) and DP 250 (pore is filled with polymer).*

assemblies can be tuned correspondingly. In addition, unlike regular porous membranes,[25] a self-assembled membrane can potentially be redispersed, cleansed from foulants, and re-assembled,[26-28] thus improving the lifetime of the material.

In previous work, we demonstrated that silica nanoparticles grafted with short polymer brushes can form robust nanoporous membranes via reversible nanoparticle assembly in organic solvents and in water, due to electrostatic and hydrophobic interactions, respectively.[26] We also reported the preparation of charged nanoporous membranes by self-assembly of HNPs functionalized with polyelectrolyte copolymer brushes.[29] We demonstrated that the pore sizes in these membranes undergo changes of up to 40% in response to changes of the ionic strength of the salt solution. We rationalized this behavior by postulating that polymer brushes in the interstitial spaces between HNPs change their conformation similar to polymer brushes grafted inside the nanopores of preformed porous solids.

This work focuses on HNP membranes that are responsive to changes in temperature. Temperature is a stimulus that is easy to apply and thermoresponsive components are widely available. Specifically, we used HNPs carrying brushes of poly(N-isopropylacrylamide) (PNIPAM). PNIPAM is one of the most commonly used thermoresponsive polymers due to its accessibility and reversible response in a physiological temperature range.[30] The temperature response of PNIPAM is particularly attractive in applications where controlled permeability is desired, such as nanofluidic valves or nanoporous membranes.[31]

In aqueous media below ~32 °C (the lower critical solution temperature, LCST),[32] PNIPAM exists in a

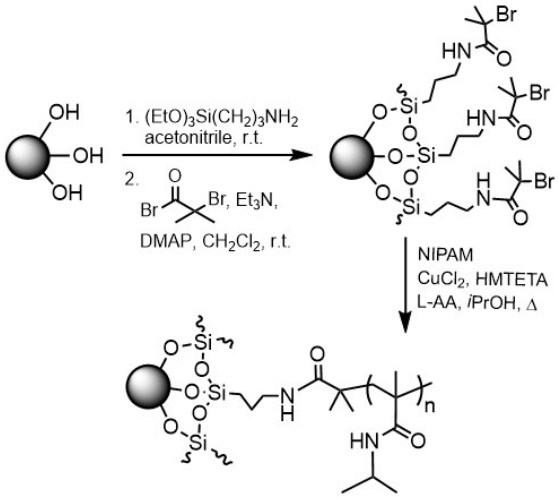

Scheme 1. *Preparation of PNIPAM polymer-brush silica nanoparticles.*

Table 1. *Polymer brushes investigated in this study.*

Brush	Polymerization time, min	DP
short	30	80
medium	60	250
long	120	450

hydrated relaxed coil conformation; at higher temperatures, the solubility of the polymer dramatically decreases, causing it to collapse into a globular conformation.[33] The transition temperature of bulk PNIPAM is largely independent of molecular weight, tacticity, or concentration.[34] Parameters that directly affect polymer-solvent interactions (e.g., solvent species and ionic strength) can affect the transition temperature.[35]

The behavior of PNIPAM brushes on surfaces has been extensively studied.[36] In particular, spherical silica nanoparticles grafted with PNIPAM brushes

showed phase transition in the range similar to that of PNIMAP in solution,[37] with grafting density affecting the LCST and the sharpness of the temperature response.[38]

Previously, we reported on the preparation of porous films of silica nanoparticles functionalized with PNIPAM polymer brushes.[23] In that material, PNIPAM was grafted from the silica particles *after* self-assembly of the particles into a solid membrane whose porosity stems from the network of interconnected three-dimensional voids between the silica particles.[24] These PNIPAM-modified colloidal films showed two types of responsive permeability behavior, depending on the length of the grafted polymer chains. Shorter PNIPAM brushes collapsed at temperatures above the LCST, thus opening the pores. Longer PNIPAM brushes formed a hydrophobic gel inside the nanopores at temperatures above the LCST and prevented water permeation. This behavior is consistent with the properties of responsive polymers under confinement,[39-42] where polymer response also depends on the degree of polymerization.

In this work, we describe the preparation of colloidal temperature-responsive membranes by self-assembly of pre-prepared PNIPAM-covered HNPs. These nanoporous membranes are flexible and reusable with pore sizes that can be easily controlled by the size of the building blocks.[34,43] We assembled the PNIPAM-HNPs into thin films through pressure-driven deposition of nanoparticle suspensions, determined the permeability of these membranes at different temperatures, and measured their effective pore sizes. Molecular dynamics computer simulations reveal the polymer configurations inside these materials and help rationalize the observed temperature response.

Materials and Methods

Materials. Anisole, 3-aminopropyltriethoxysilane (APTES), triethylamine, 2-bromoisobutyryl bromide, N-isopropylacrylamide (NIPAM), 1,1,4,7,10,10-Hexamethyl triethylenetetramine (HMTETA), monodisperse dextrans of various molecular weights, and polystyrene spheres were purchased from Sigma Aldrich. 4-dimethylaminopyridine (DMAP) and tethraethoxysilane (TEOS) were purchased from Alfa Aesar. Dichloromethane (DCM), isopropanol, methanol, L-ascorbic acid (L-AA), dimethylformamide (DMF) and ammonia hydroxide solution were purchased from Fischer Chemicals. Copper (II) chloride dihydrate was purchased from Acros Organics.

Measurements. Scanning electron microscopy (SEM, FEI Nova NanoSEM 630; particles were imaged in the low-vacuum mode) and transmission electron microscopy (TEM, JEOL JEM-1400) were used to image the HNPs. Thermogravimetric analysis of polymer-modified particles was conducted using a SSC 5200 thermogravimetric analyzer (Seiko) at a heating rate of 10 °C/min from room temperature to 800 °C. A Branson 1510 sonication bath was used for all sonications. UV/Vis measurements were performed using an Ocean Optics USB4000 instrument.

Preparation of silica particles. Silica nanoparticles (SNPs) were prepared using the Stöber method.[44] The size of nanoparticles was determined by TEM to be 247±17 nm.

Grafting of polymerization initiation sites. ATRP sites were prepared in two steps using previously described procedures.[23,36,37] In the first step, primary amines were grafted on the surface to facilitate the addition of initiator sites as follows: 1 mL of APTES was added to a suspension of ~2 g of Stöber silica particles in 15 mL of dry acetonitrile. The reaction flask was immersed in an oil bath at 60 °C and the reaction mixture was stirred for 6 hours. Aminated particles were collected by centrifugation, washed at least three times with acetonitrile and dried. In the second step, polymerization initiator sites were grafted to the surface of the silica particles as follows: to a prepared suspension of ~1 g of aminated silica particles in 50 mL anhydrous DCM we added 40 mg (0.3 mmol) of DMAP, 2.09 mL (15 mmol) of triethylamine and 1.61 mL (13 mmol) of 2-bromoisobutyryl bromide. The reaction mixture was stirred at room temperature for 24 hours. The resulting particles were collected by centrifugation, washed at least three times with DCM and then dried. Successful surface modification after each step was confirmed using thermogravimetric analysis (TGA).

Polymerization. Polymer brushes were grafted through activators regeneration by electron transfer atom-transfer radical polymerization (ARGET-ATRP).[45] In a typical polymerization procedure, 500 mg of silica particles with initiator sites was combined with 1.2 g (10.6 mmol) of NIPAM in 2.4 mL isopropanol and 50 μL of $CuBr_2$ and HMTETA stock solution (1:10 molar ratio, respectively, with $CuBr_2$ concentration of 200 mM) in DMF. Then, the reaction mixture was degassed by two freeze-pump-thaw cycles and 8 mg (45 μmol) ascorbic acid in 1 mL of DMF was added to the mixture. The reaction was left stirring at 60 °C under nitrogen atmosphere, with polymer length controlled by allowed reaction time (see Table 1). The final "hairy" particles were collected by centrifugation, washed at least three

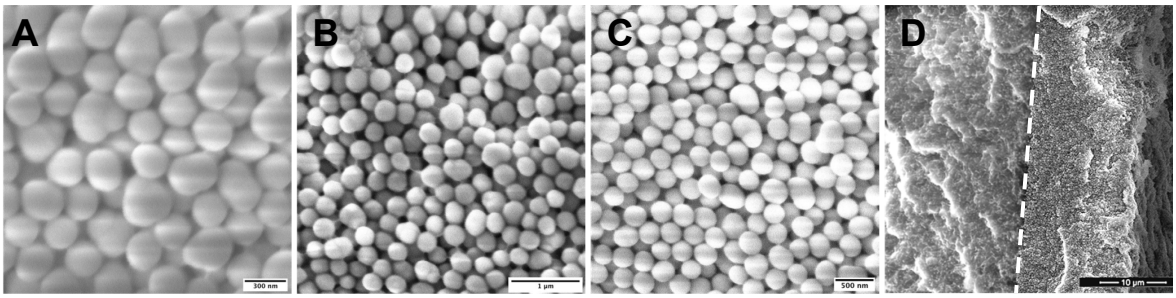

Figure 2. *(A-C) SEM images of HNP-PNIPAM membranes made with polymer brushes of DP=80 (A), DP=250 (B), and DP=450 (C). (D) A representative SEM image of a cross-section of an HNP-PNIPAM membrane (DP=250). The nylon support is on the left and the membrane is on the right in the image, the interface is marked with a dashed line. Scale bars are as shown.*

times with acetonitrile, and dried. The degree of polymerization (DP) was calculated using TGA (**Figure 7S** in the Supporting Information). TEM images of HNPs with different DP are shown in **Figure 1**.

Membrane preparation. A modified 10 mL dead-end filtration cell (Sterlitech Corporation) was used to prepare and study the HNP membranes. The membrane was prepared through pressure-driven deposition of a suspension of ~12 mg of nanoparticles in 10 mL 50% acetonitrile/H_2O onto a nylon support with a nominal pore size of 0.22 μm (Tisch Scientific, North Bend, OH; pore size determined using bubble point method) at room temperature. The applied pressure was set to 1 bar. The average membrane thickness was 60 micrometers, as measured using a digital micrometer. SEM images of HNP membranes with different DP are shown in **Figure 2**.

Membrane testing. Water with a resistivity of 18 MΩ cm was used in the preparation of all solutions and in all water flow experiments. Water flow was measured by driving pure water through the membrane and weighing collected fractions over time. The desired temperature was achieved and maintained by heating water directly in the cell, via a thermocouple installed in the water chamber. Once the water reached the desired temperature, an air pressure of 1 bar was applied and the flux through the membrane was recorded. The water flow and membrane thickness data are given in the **Supporting Information**.

The pore size cutoff was determined using suspensions of polystyrene spheres in water (40 μL of 0.2% by weight solution diluted with water to 4 mL). The solution was driven through the membrane at an applied pressure of 1 atm and the amount of permeate was determined spectrophotometrically at a wavelength of 240 nm for polystyrene spheres.

Modeling. The PNIPAM polymer brushes were represented via a coarse-grained model that accounts for solvent effects implicitly.[46] Polymers were modeled as linear chains of beads representing one NIPAM monomer that interact pairwise through the Lennard-Jones potential:

$$U(r) = 4\varepsilon\left[\left(\frac{\sigma}{r}\right)^{12} - \left(\frac{\sigma}{r}\right)^{6}\right] \qquad (1)$$

We set σ = 0.59 nm and ε is chosen in the range 0.1-3.1 kJ/mol to represent different effective temperatures. For this value of σ, the brush height of our model at ε = 0.1 kJ/mol matches results by Leonforte and coworkers[47] for low effective temperature. Our model parameterization procedure is described in detail on pages S-1 and S-2 of the **Supporting Information**. Interactions were cut and shifted to zero at a distance of 2.5σ = 1.475 nm. Adjacent beads along the chain were bound by a harmonic potential:

$$U = \frac{1}{2}k(r - r_0)^2 \qquad (2)$$

where k = 1000 kJ/(mol nm^2) and r_0 = 0.59 nm. No bond angle or dihedral potentials were used. Lennard-Jones interactions between bonded particles were set to zero. A more detailed description of the parameterization of the model is given in the **Supporting Information**.

Silica nanoparticle cores were modeled as rigid bodies consisting of 6839 particles that are placed in a close-packed arrangement on the surface of a sphere with 80 nm diameter, resulting in a grafting density of 0.35 nm^{-2}. In all our simulations, we considered a single nanoparticle core size (80 nm diameter) covered with brushes of polymer with three different numbers of monomers (i.e., degrees of polymerization): DP 50, DP 80, and DP 145. A HNP with DP 145 has a total of approximately 1 million particles. A snapshot of a model HNP with DP 50 is shown in **Figure 3**.

In our model, different solvation states of the polymer brush (from well-solvated, swollen brushes to completely desolvated, collapsed brushes) were

modeled by appropriate choices of the monomer interaction strength ε: At small values of ε, attractive interactions between monomers are weak and the polymers adopt open coil structures, resulting in swollen brushes. This behavior is observed for PNIPAM below the LCST. At larger values of ε, monomers attract each other strongly and polymer brushes collapse, corresponding to the behavior of PNIPAM above the LCST. In our simulations, we therefore used the interaction parameter ε as a proxy for the *effective* temperature of a PNIPAM brush in water; the physical temperature in our simulations is set to 300 K and is held fixed throughout this work.

While we did not attempt to accurately map temperature to the interaction parameter ε, we estimated the value ε_0 that best corresponds to the LCST of our PNIPAM model. To this end, we calculated potentials of mean force (PMF) of two HNPs with DP 50 brushes for various values of ε, as illustrated in **Figure 4**. While the PMF for ε = 0.7 kJ/mol is repulsive, PMFs for $\varepsilon \geq 0.7$ kJ/mol display a free energy well indicative of strong attractive interactions. We therefore estimate the LCST of our model to occur at $\varepsilon_0 \approx 0.7$ kJ/mol, which therefore corresponds to an effective temperature of 32 °C. Based on this estimate and by comparison with a previous model for PNIPAM,[47] we can furthermore estimate that values of $\varepsilon \approx 0.1$ kJ/mol correspond to temperatures of 20 °C or lower, and values of $\varepsilon > 2$ kJ/mol correspond to temperatures of 50 °C and above.

Additional computational methods are provided in the **Supporting Information**. All MD simulations were performed with a time step of 10 fs using NVT/NPT integrators implemented in HOOMD-blue[48] on NVIDIA Tesla V100 GPUs at the Center for High-Performance Computing at the University of Utah.

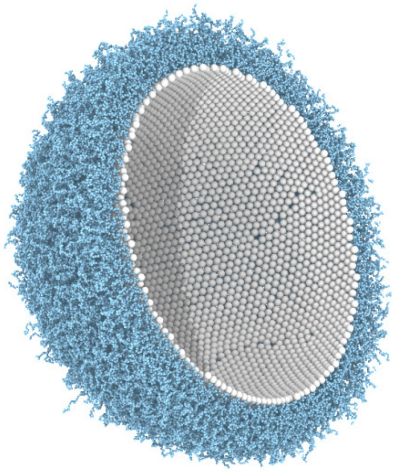

Figure 3. *A snapshot from MD simulations, showing a cross-section of a HNP with DP 50 at low effective temperature (ε = 0.1 kJ/mol). Grafting sites are shown in grey color, polymer chains are colored blue.*

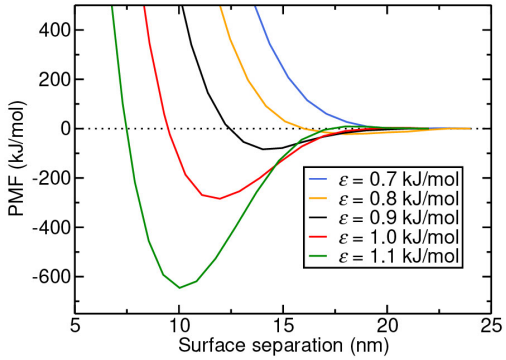

Figure 4. *Potentials of mean force (free energy) for two HNPs with DP 50 as a function of surface-to-surface distance, for several values of the polymer interaction parameter ε.*

Results and discussion

Preparation of nanoparticles. Polymer-brush silica nanoparticles were prepared as shown in **Scheme 1**. We used silica nanoparticles with an average diameter of 247±17 nm, grafted the ATRP initiation moieties in two steps by amination and consequent acylation,[34] and formed PNIPAM polymer brushes on silica surface using the ARGET-ATRP technique,[45] which allows controlling the polymer length by the polymerization time. For the PNIPAM polymer brushes in this work, we prepared HNPs with three different degrees of polymerization (DP): 80, 250, and 450 (**Table 1**). Below, we will refer to these brushes as "short", "medium" and "long", respectively. The resulting HNPs had different physical appearance after drying: particles with short brushes behaved similarly to unmodified silica particle while particles with long brushes formed gel-like solids. This observation is in agreement with the effects of polymer length and grafting density on nanocomposite behavior and mechanical properties reported in the literature.[49]

We characterized the HNPs with different brush thicknesses by TEM, as shown in **Figure 1**. In these images of dry particles, the polymer brushes are well visible, particularly in the regions around the points of contact between the pairs of HNPs. Effects of different brush thickness on the spatial arrangements of HNPs can also be inferred from

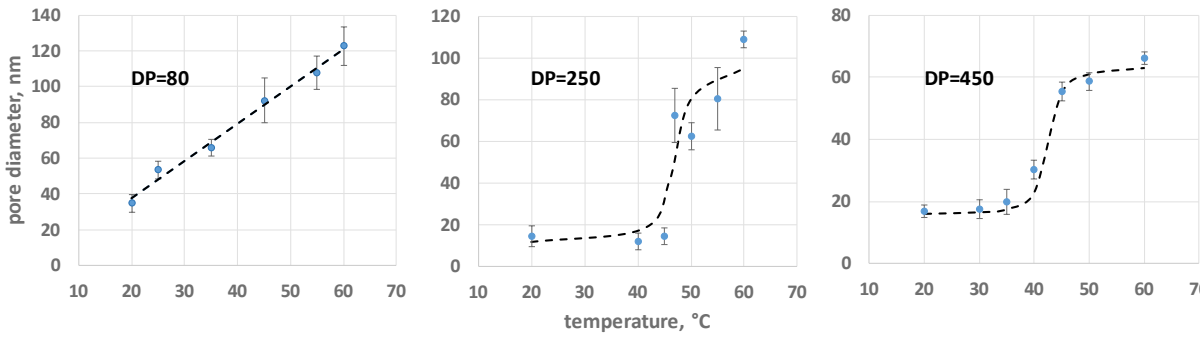

Figure 5. *Average pore diameters calculated using the water flux data. Dashed lines are visual aids only. Error bars are based on triplicate measurements for each system.*

these images: For HNPs with "short" brushes (**Figure 1a**), spaces (i.e., pores) between close-packed triplets of HNPs are void of polymer; HNPs with "long" brushes (**Figure 1c**) form pores that appear to be entirely filled with polymer.

Membrane preparation. PNIPAM-HNP membranes were prepared using pressure-driven deposition of nanoparticles at room temperature to form thin films on top of porous nylon supports, as described in the Methods section. We used a water/acetonitrile solvent mixture for the deposition as PNIPAM NHPs cannot be easily dispersed in water. Top-view SEM images of prepared membranes are shown in **Figure 2A-C**. HNPs in the membranes are disordered. Regions of local order are apparent but are limited in size to a few particle diameters. The side-view of a membrane with DP=250 is shown in **Figure 2D**. The membrane is attached tightly to the nylon support, which, in combination to the polymer-polymer interdigitation, might explain the mechanical robustness of the membranes.

Temperature-responsive behavior and pore size of HNP membranes. We measured the flow of water through the membranes as a function of temperature between 20 and 60 °C. An effective pore size was then calculated based on the water flux data (see **Table 1S** of the Supporting Information) using standard equations of fluid mechanics for porous particle beds. Specifically, the effective pore diameter D_{flux} was estimated using the Kozeny-Carman equation,[50]

$$D_{flux}^2 = 16K\kappa/\varepsilon \qquad (3)$$

where K=4.8 is the Kozeny constant,[51] ε=0.36 is the membrane porosity for randomly packed spheres,[52] and κ is the permeability of the membrane, which we determined from the water flux J through the membrane using Darcy's law:

Table 2. *Estimated average pore diameters from water flux and size cutoff, at room temperature (RT) and 60°C (All values are in nanometers.)*

Brush	D_{flux}		D_{cutoff}	
	RT	60 °C	RT	60 °C
short	30	100	30-50	50-100
medium	20	90	<30	<30
long	10	60	<30	<30

$$\kappa = J\mu L/\Delta P \qquad (4)$$

Here, μ=1.00 mPa·s is the viscosity of water, L is the thickness of the membrane, and ΔP=*1 atm* is the applied pressure. The plots of calculated pore diameters for membranes prepared from HNPs with three different polymer brush lengths as a function of temperature are shown in **Figure 5** and are listed for room temperature and 60 °C in **Table 2**.

All membranes displayed increasing water flux and pore size with increasing temperature. The magnitude and specific pattern of the temperature response, however, depended on the PNIPAM brush thickness. Membranes with short brushes showed a nearly linear increase in the pore diameter with temperature, while membranes with medium and long brushes displayed a sigmoidal response, resembling the gated behavior associated with typical PNIPAM materials.[53] Bittrich *et al*. have observed a similar effect of the polymer thickness on the temperature response using ellipsometry as the probing method.[54]

The transition temperatures for the medium and long brush membranes (as estimated from inflection points in **Figure 5**) fall between 40 and 50 °C, which is noticeably higher than the typical PNIPAM LCST of 32 °C.[32] The range of observed pore diameters also differed markedly between membranes with different brush thickness. With increasing

temperature, the pore diameter changed from ca. 30 nm to 120 nm for membranes with short brushes, from ca. 20 to 110 nm for medium brushes, and from ca. 20 to 60 nm for membranes with long brushes, based on the water flux measurements in the tested range. We thus observe that the change in pore diameter over the given temperature range is smallest for the HNP membranes with the longest polymer brushes. A similar observation was reported for polyelectrolyte brushes, where longer brushes showed smaller magnitude of change in response to the changing concentration of electrolyte solution.[29] We return to this observation below, in the discussion of our simulation results.

We further investigated the effective pore diameters in PNIPAM-HNP membranes by filtration cutoff experiments using polystyrene spheres of 30, 50, and 100 nm diameter. Membranes with short brushes allowed for the passage of 30 nm spheres and retained 50 nm and 100 nm spheres at room temperature; at 60 °C, the membrane was permeable to both 30 and 50 nm spheres, but not to 100 nm spheres. We thus estimate the effective pore diameter D_{cutoff} as 30-50 nm at room temperature and as 50-100 nm at 60 C for membranes with short brushes. For comparison, three spheres in a close-packed arrangement form a concave triangular pore whose size can be estimated by the diameter of a circle that fits inside. For 250 nm particles, the diameter of this circle is ~39 nm. Similarly, four close-packed 250 nm particles in a square arrangement produce a pore with a circular diameter of ~62 nm.

Consistent with pore sizes estimated from flux measurements, membranes with medium and long brushes have a smaller size cutoff for filtration. Both types of membranes retained polystyrene spheres of all sizes for an estimated effective pore diameter of <30 nm at all temperatures. To confirm that the retention of polystyrene spheres is the result of pore rejection and not of adsorption on the HNPs, we centrifugated a suspension of HNPs and polystyrene beads and monitored the concentration of polystyrene beads in the supernatant.[55] This experiment confirmed that polystyrene beads do not adsorb on HNPs due to particle-particle interactions in solution.

As is evident from **Table 2**, pore diameters estimated by water flux are significantly larger than filtration cutoff sizes for membranes with medium and long brushes at 60 °C. We speculate that this discrepancy is due to the different nature of the two pore size measurements. While we would expect water flux and size-cutoff experiments to give comparable results for membranes of randomly close-packed spherical particles, the presence of polymers in the pores of such membranes can create barriers that effectively block the passage of larger solid objects while having little effect on water flux. The filtration cut-off size of HNP membranes may be further decreased by pore tortuosity. Indeed, the tortuous pore path formed in close-packed assemblies of nanoparticles may lead to retention of permeating objects much smaller than the pore opening.[56-58]

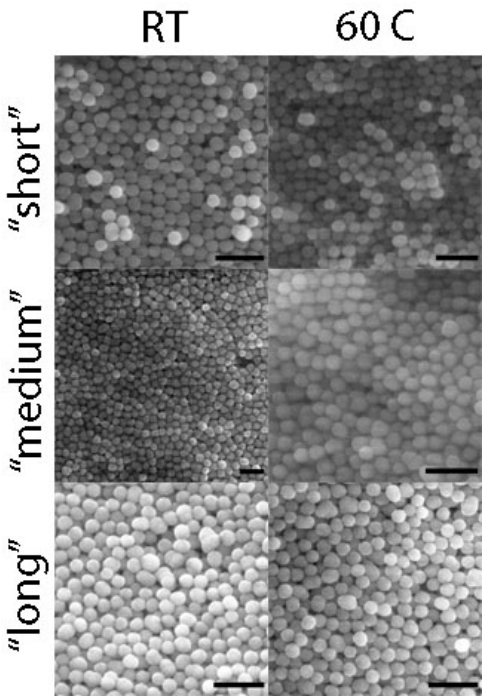

Figure 6. *SEM top-view images of PIMIPAM-HNP membranes before and after exposure to 60 °C water. Scale bars are 1 μm.*

Mechanical stability of the membranes. One potential caveat of using a temperature-responsive polymer as a major component of a self-assembled membrane held together by non-covalent interactions is that such a membrane might undergo large-scale changes in dimension or morphology as a consequence of conformational changes of the polymer. In addition to affecting the pore size, the expansion or contraction of the polymer chains located between the particles may in principle lead to the swelling or contraction of the entire membrane.

We examined if the PNIPAM-HNPs membranes undergo any dramatic structural changes as the result of temperature cycling between room temperature and 60 °C. We did not observe any dimensional changes in these membranes using optical microscopy and SEM (**Figure 6**). The

membranes did not show any significant structural defects before or after exposure to high temperatures, and no qualitative change in the packing of HNPs on the membrane surface was observed, indicating excellent membrane stability. Moreover, membranes that had been subjected to the low-vacuum conditions during SEM imaging could be rehydrated and reused without noticeable change in performance.

We speculate that the observed mechanical behavior results from the polymer brushes acting as "molecular glue" in which the strong interchain and interparticle interactions are induced during the membrane formation and solvent evaporation, effectively locking the particles in place. We conducted a simple experiment to probe the importance of the self-assembly and solvent evaporation for the mechanical stability and performance of the membranes. We prepared two membrane samples from a single batch of medium brush HNPs using two different preparation methods: (1) The membrane was prepared by compressing dry HNPs using a hydraulic press at 5,000 psi; (2) the membrane was self-assembled from the colloidal HNP suspension as described above. Both membranes were then submerged in water at room temperature. While the self-assembled membrane was stable, the pressed membrane immediately disintegrated. This experiment suggests marked differences between the configurations of polymer chains in the pressed and self-assembled membranes; it indicates that polymer chains grafted from different HNPs entangle and strongly interact during self-assembly in solution, providing the "molecular glue" responsible for the mechanical stability observed in our experiments.

Modeling of PNIPAM-HNP membranes. To shed light on the polymer configurations and temperature response of our HNP membranes, we performed molecular dynamics (MD) simulations of a coarse-grained model of HNPs (see Methods). Due to the large number of beads used to represent a single HNP, the computational cost of simulating large numbers of HNPs or even an entire HNPs membrane is prohibitively large. Instead, we focused on arrangements of small numbers of HNPs that form important structural elements of close-packed arrangements of spherical particles: triangular arrangements of three close-packed HNPs and square arrangements of four HNPs. The space between HNPs in the triangular motif is the smallest pore that appears in crystalline close-packed structures (face-centered cubic or hexagonally close-packed). A hypothetical close-packed crystalline

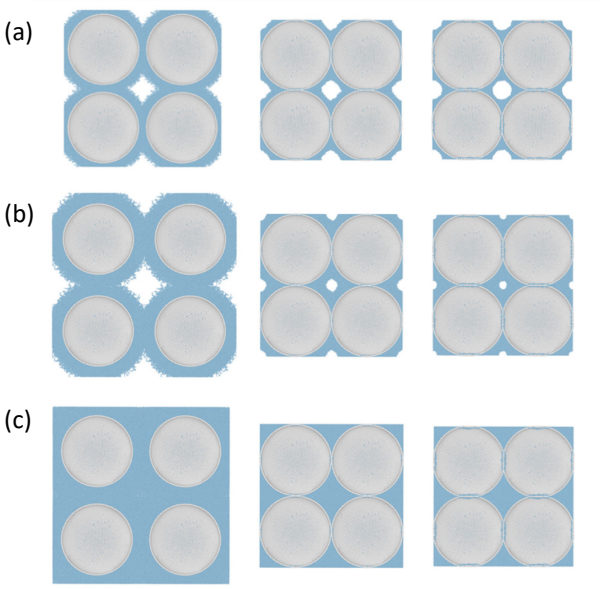

Figure 7. *Snapshots from MD simulations at fixed pressure, showing cross-sections of a square pore motif formed by four HNPs with different degree of polymerization (a) DP 50, (b) DP 80, (c) DP 145. Particles representing the nanoparticle surface are shown in grey color, polymers are shown as blue chains. Effective temperature (see Methods) increases from left to right: (left) ε=0.1 kJ/mol, (center) ε=1.5 kJ/mol, (right) ε=3.1 kJ/mol.*

membrane of HNPs can be viewed as a network of octahedral and tetrahedral voids connected by such triangular pores. The square motif of four HNPs is found at the center of octahedral voids in close-packed crystals and thus represents the largest empty space in a hypothetical close-packed crystalline membrane of HNPs. Of course, HNP membranes in our experiments are not crystalline (see **Figure 4**) and therefore have a lower packing fraction and, on average, larger pore sizes than those in crystalline packings. We nevertheless expect that the two HNP motifs investigated here are representative for the pore configurations in our amorphous membranes.

We simulated model HNPs with 80 nm core diameter and brushes consisting of polymers with DP 50, 80 and 145. Although our model HNPs are somewhat smaller than their experimental counterparts, they cover a similar range of polymer lengths relative to the particle diameter. We equilibrated triangular and square HNP motifs at 1 atm pressure and low effective temperature (i.e., weak monomer interaction strength ε), approximating the conditions at which HNP membranes are fabricated in our experiments. Starting from these equilibrated configurations, we then run molecular dynamics while increasing the

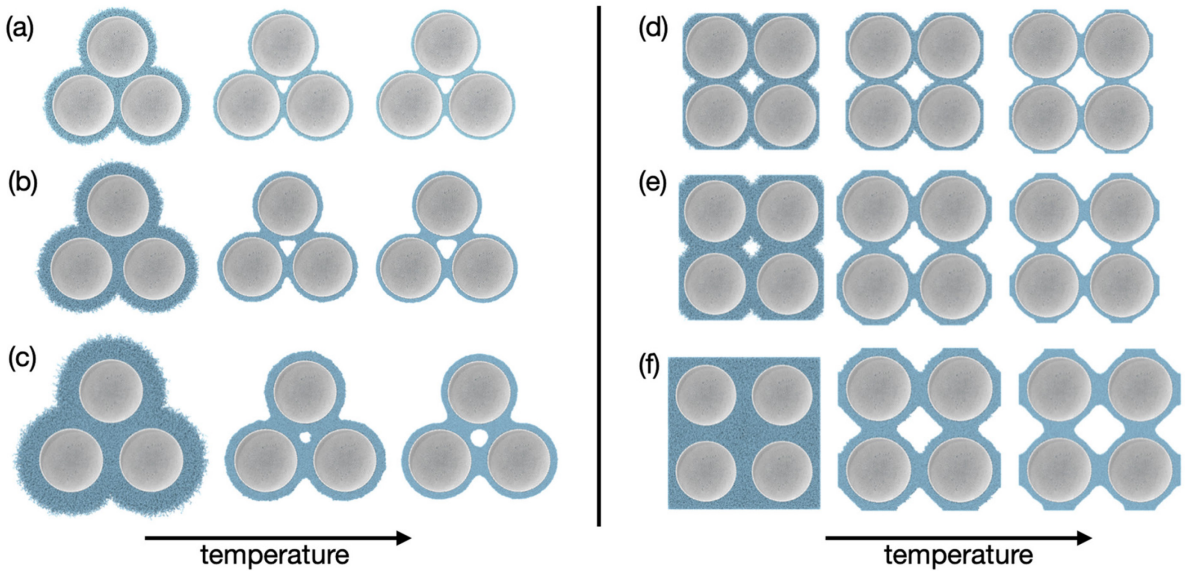

Figure 8. *Snapshots from MD simulations with fixed HNPs distance, showing cross-sections of the pore motif formed by HNPs. Left: Triangular pore motif formed by three HNPs. Right: Square pore motif formed by four HNPs. HNPs have different degree of polymerization: (a) and (d) DP 50, (b) and (e) DP 80, (c) and (f) DP 145. Particles representing the nanoparticle surface are shown in grey color, polymers are shown as blue chains. Effective temperature (see Methods) increases from left to right: (left) ε=0.1 kJ/mol, (center) ε=1.5 kJ/mol, (right) ε=3.1 kJ/mol.*

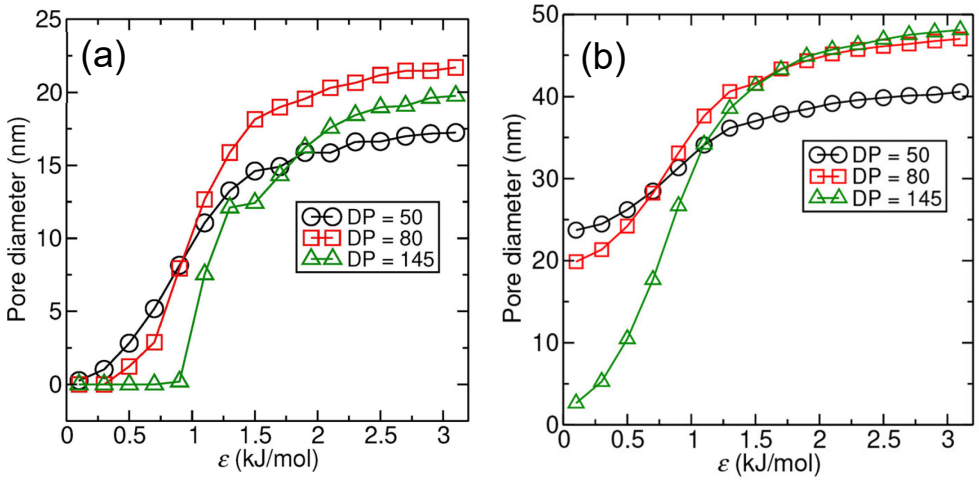

Figure 9. *Plot of the pore diameter measured in simulations for different degrees of polymerization, as a function of monomer interaction strength (corresponding to effective temperature). (a) Triangular pore. (b) Square pore.*

effective temperature in the simulations and measuring the size of the pore formed by polymer chains in the void space between HNPs (see **Supporting Information**).

The pores' response to temperature changes in our simulations shows a striking dependence on external conditions. When the pressure is held fixed at 1 atm throughout the simulations, pore sizes either stay approximately constant (for short polymer brushes) or decrease (for medium and long brushes) when the temperature is increased (see **Figure 7**). This behavior can be explained by considering interactions between the polymer brushes. At low temperature, PNIPAM chains are well solvated and PNIPAM brushes swell. Under these conditions, HNPs possess effectively repulsive interactions. At higher temperatures, above the LCST, PNIPAM chains collapse, consistent with effectively attractive polymer brush interactions. Under these conditions, HNPs will approach one another (up to the point of

contact in our simulations) to increase the number of favorable polymer-polymer interactions and reduce the interface area of polymer and water. As a result, the space between HNPs that is void of polymers (i.e., the pore) shrinks. Importantly, these changes in polymer structure and HNP distance should result in a *decrease* of water flux and cut-off filtration size—in direct opposition to our experimental results, which show increasing effective pore sizes with increasing temperature for all systems. We conclude that constant-pressure simulations, although apparently consistent with our experimental setup, do not accurately model structural changes in our membranes. TEM images of HNP membranes before and after heating to 60˚C (**Figure 6**) support this conclusion, as no significant changes in HNP distance or membrane dimensions are observed. In addition, if HNP distances decreased markedly upon heating as suggested by our constant-pressure simulations, HNP membranes could develop obvious cracks. However, we did not observe any signs of membrane cracking in any of our images.

The temperature response of our membranes is qualitatively reproduced in simulations where the distance between HNPs was fixed, as illustrated in **Figure 8**. While polymers extend well into the space between HNPs (and even fill that space entirely for triangular pores or long brushes) at low temperature, polymer brushes retract towards the surface of HNP cores as temperature is increased, thereby opening large pores, in agreement with our experiments. This result indicates that distances of HNPs in our membranes are insensitive to the solvation state of the polymer brushes as controlled by temperature. This conclusion is consistent with the observation that self-assembled membranes in water at room temperature are mechanically stable (as described in the previous section), even though PNIPAM brushes are swollen under these conditions and polymer interactions are effectively repulsive. We suggest that HNPs closely approach their nearest neighbors during membrane assembly and become irreversibly bound via strong van der Waals interactions between silica cores. This hypothesis is supported by TEM images of isolated HNPs (**Figure 1**): neighboring particles in these images appear to have surface-to-surface distances on the order of a few nanometers.

Pore sizes as a function of temperature, as measured in our simulations, are shown in **Figure 9**. Our method of measuring pore size (see **Supporting Information**) is likely more closely related to filtration cutoff size than to pore size determined via water flux, in particular at low temperature: While well-solvated polymer chains that fill the space between HNPs (and therefore are assigned a pore size of zero in our simulations) likely block the passage of large solid particles, water can still flow through. The curves in **Figure 9** have sigmoidal shape for both pore geometries and all polymer lengths—the linear temperature response observed in experiments of short-brush HNPs (**Figure 5**, left panel) is not found in simulations. The inflection points of these curves are at $\epsilon \approx 1.0$ kJ/mol (or even larger values for long brushes and triangular pores), which corresponds to a temperature that is larger than the estimated LCST of our model ($\epsilon \approx 0.7$ kJ/mol). This result agrees with our experiments, where HNP membranes also show the strongest temperature response at temperatures above the LCST. We rationalize this result based on the temperature dependence of polymer brush height (**Figure 1S**), which also has its inflection point at values of ϵ that are larger than the corresponding value at the LCST: while effective attractions between polymer chains become sufficiently large for bulk phase separation at the LCST, chain configurations (and, therefore, pore sizes) change most dramatically at somewhat higher temperatures.

Next we turn our attention to the configurations adopted by polymer chains in the space between pairs of interacting HNPs. Polymer chains in dense brushes like the ones used in our work are expected to adopt significantly stretched configurations (compared to random coils adopted by isolated

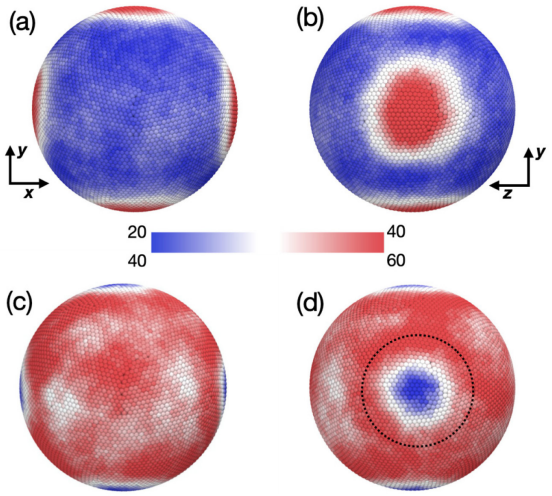

Figure 10. *Map of polymer angles (as defined in Figure 6S) on the surface of HNPs in a square lattice. (a) and (b): low effective temperature, ε = 0.1 kJ/mol. (c) and (d): high effective temperature, ε = 3.1 kJ/mol. Color scale indicates different angle ranges: (a) and (b): 20°-40°; (c) and (d): 40°-60°. Angles have been averaged over all polymers grafted within a 10 nm radius.*

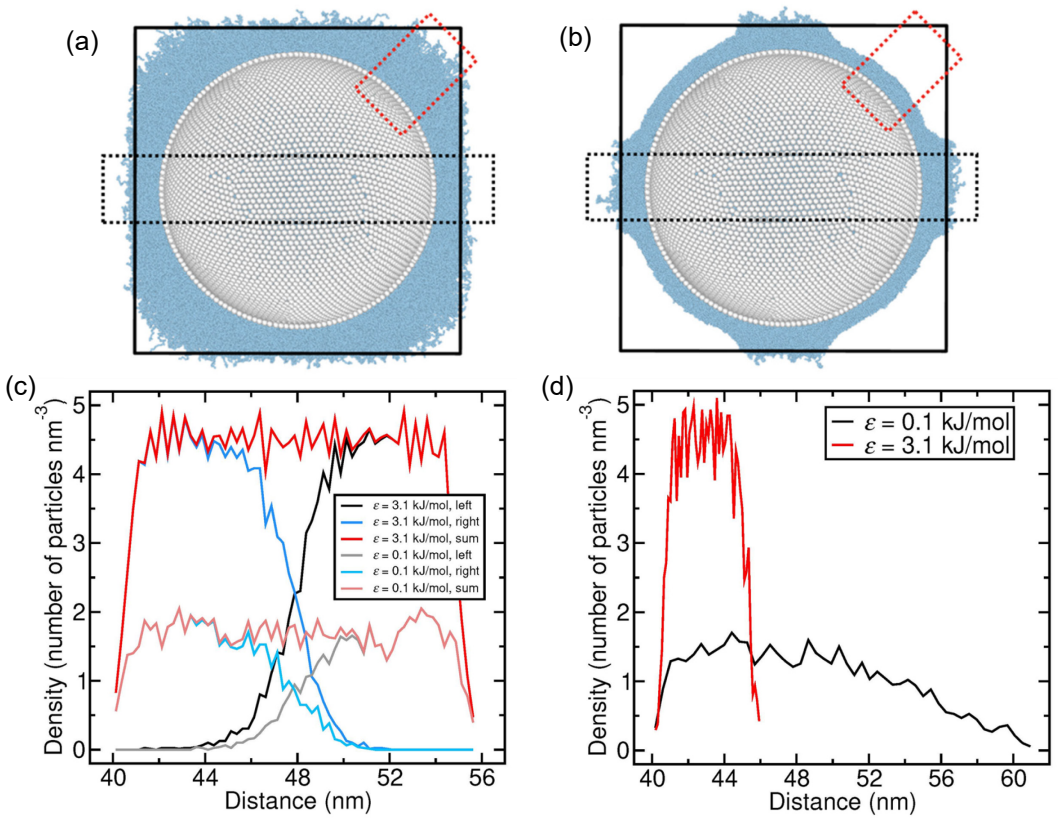

Figure 11. *Cross-sections of model HNPs in a square lattice, with DP 80 at (a) low (ε = 0.1 kJ/mol) and (b) high (ε = 3.1 kJ/mol) effective temperature. (c) Polymer density (number of monomers per nm^3) as a function of distance from the center of the HNP (HNP radius is 40 nm), measured within cylindrical regions outlined with black dashed lines in panels (a) and (b). Density of polymers grafted to opposing HNPs ("left" and "right") and total density ("sum") are shown as separate curves. (d) Polymer density (number of monomers per nm3) as a function of distance from the center of the HNP (HNP radius is 40 nm), measured within cylindrical regions outlined with red dashed lines in panels (a) and (b).*

chains).[59] Between two interacting HNPs, however, chain configurations might be significantly altered as polymers from different particles interdigitate. The polymer structure between HNPs is key for understanding the mechanical properties and temperature response of HNP membranes.

For this analysis, we focus on the square pore geometry and medium polymer length (DP 80, **Figure 8e**). As a point of reference, we first analyze the polymer density and brush thickness in isolated HNPs at low and high temperature (ε = 0.1 kJ/mol and ε = 3.1 kJ/mol, respectively), as shown in **Figure 12**. In its fully solvated state (**Figure 12a**), the brush extends approximately 20 nm from the HNP surface; at high effective temperatures (**Figure 12b**), the brush collapses to a height of approximately 6 nm, with a maximum brush density that is approximately three times larger than that of the swollen brush.

For interacting HNPs in a square pore (**Figure 11**), we find that the parts of the polymer brushes that are not near points of contact between different HNPs (e.g., regions marked with red dashed lines in **Figure 11 a** and **b**) have brush densities and brush heights that are similar to their isolated counterparts (see **Figure 11d** and **Figure 12c**, "upper-right"). Near points of contact between different HNPs (e.g., regions marked with black dashed lines in **Figure 11a** and **b**), polymer brushes have markedly different structures. We first discuss the low-temperature regime. The surface-to-surface distance between HNPs in the square arrangement is approximately 16 nm, which is smaller than the brush height (20 nm) of an isolated brush. Polymer brushes from opposing HNP surfaces therefore compete for space and must either adopt significantly compressed configurations, resulting in a larger polymer density than in other parts of the brush, or bend away from the line of contact between the two HNPs. We find that both scenarios apply: the polymer chains between HNP surfaces have approximately 40% larger density than isolated brushes (see **Figure 12c**), but only extend approximately 10 nm from the HNP surface they are bound to. This implies that polymer chains close to

the line of contact between HNPs do not extend radially from the surface on average but bend away to form a vortex-like structure. Similar behavior has been found in much smaller nanoparticles covered with short alkane chains.[60,61]

The vortex-like structure of polymers around the point of contact between pairs of HNPs can be visualized by measuring the angle between a vector connecting the head and tail of a given polymer chain with the radial vector at the grafting point of the polymer, as illustrated in **Figure S1**. In **Figure 10** panels (a) and (b), we show a spatial map of the angle of polymer chains grafted on an HNP in contact with four other HNPs on a square lattice. The angle map shows that polymers in the region around lines of contact with other HNPs adopt significantly larger angles than polymers grafted further away.

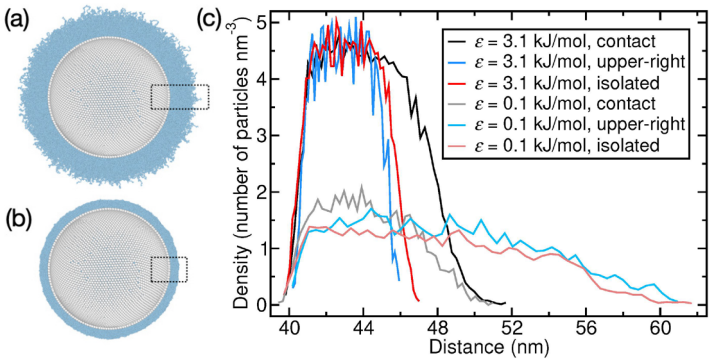

Figure 12. *Cross-sections of isolated model HNPs with DP 80 at (a) low (ε = 0.1 kJ/mol) and (b) high (ε = 3.1 kJ/mol) effective temperature. (c) Polymer density (number of monomers per nm^3) as a function of distance from the center of the HNP (HNP radius is 40 nm), for HNPs shown in panel a (light red curve) and panel b (dark red curve). Density profiles for interacting HNPs are also shown (compare **Figure 11**).*

While polymers bend away from regions of contact at low temperatures, a strikingly different behavior is observed at high temperatures, when polymers have strong attractive interactions and brushes are dense. In this regime, we observe the formation of polymer "bridges" that connect neighboring HNPs, as shown in **Figure 11b** and **Figure 8**. The surface-to-surface distance between HNPs in our square configuration (16 nm) is larger than twice the height (2×6 nm) of an isolated collapsed brush. Driven by strong polymer interactions and the tendency to minimize the area of the water-polymer interface, polymer chains extend and "reach" across the space between HNPs to form a connection between neighboring HNPs, as shown in **Figure 11b**. Notably, the polymer density in the bridge region is not significantly lower than in regions away from the contact point (see **Figure 12c**). This contrasts with the low-temperature case discussed above, where the density in the vortex region was markedly increased. At high temperatures, polymers are fully collapsed in water with similar density to the dry bulk polymer. In this state, the polymer is essentially incompressible—any density change incurs a large free energy penalty. A dilute, swollen polymer is compressed much more easily. The stretched polymer configurations together with the unchanged density in the bridge region implies that additional polymer chains must be recruited into the bridge from surrounding areas. In other words, while polymer chains tend to bend *away* from the region of contact (vortex) at low temperatures, they tend to bend *towards* the region of contact (bridge) at high temperatures. This notion is confirmed by angle maps shown in **Figure 10**, panels (c) and (d): Polymer chains in the bridge region have significantly smaller angles on average, as they stretch towards the opposing HNP; polymer chains immediately surrounding the bridge region (dashed circle in **Figure 10d**) have larger angles, bending towards the bridge.

Finally, we turn to the question of polymer interdigitation, i. e., the degree to which polymer chains from opposing HNPs intermingle. **Figure 11c** reveals that there is a zone of approximately 5 nm thickness at the interface between two HNPs in which polymers interdigitate; these polymer chains can be seen extending across the periodic boundaries in **Figure 11a** and **11b**. Remarkably, this zone has similar dimensions at low and high effective temperature. Interactions between polymers from different HNPs in this zone are responsible for the mechanical stability of our HNP membranes. When membranes are fabricated by pressing together dried HNPs (which have polymer brush configurations similar to HNPs in water at high temperature, **Figure 12b**) this degree of interdigitation is not established, resulting in membranes that are unstable.

We note that we have not strictly confirmed that the polymer bridges observed between nearby HNPs at high temperatures are true equilibrium structures. It is conceivable that the bridge is a result of the protocol used to generate these configurations, which involves a gradual increase in effective temperature starting from equilibrated configurations at low effective temperature, where polymers interdigitate. Nevertheless, since HNP

membranes in our experiments are generated and tested using a similar protocol (assembly at low temperature, followed by heating), we expect that the observed bridge configurations occur in our experimental systems. In addition, polymers in their collapsed state show glassy behavior even on experimental time scales; true equilibrium configurations might therefore not be relevant in these HNP systems.

Conclusions

We have prepared novel nanoporous membranes by self-assembly of "hairy" silica nanoparticles carrying temperature responsive PNIPAM polymer brushes and studied these membranes both experimentally and using computer modeling. The pore diameter in these membranes could be controlled at room temperature by the polymer length. For the HNPs used (with silica core size of 250 nm), it ranged from 10 to 30 nm depending on the degree of polymerization. The water permeability of these membranes could be also controlled by temperature, with the effective pore diameter increasing by the factor of 3-6 (up to 100 nm) at 60 °C depending on the polymer length. The size selectivity of these membranes to the filtration of nanoparticles could also be attenuated by temperature. The membranes showed smaller effective pore diameters when measured using the filtration cut off, likely as the result of a stronger blocking of the nanoparticles by the polymer chains inside the pores compared to the blocking of small water molecules.

Our simulations of simple triangular and square HNP geometries give a good qualitative description of the changes in polymer configurations underlying the temperature-dependent pore sizes in our experiments. Some specific characteristics of HNP membranes are also reproduced, including the larger size of triangular pores with medium-brush HNPs compared to long-brush HNPs. However, our simulations do not offer straightforward explanations for more peculiar properties of HNP membranes, in particular the linear temperature-dependence and large pore sizes of HNP membranes with short brushes. A more accurate picture of the packing and interparticle distances of HNPs in our membranes and the resulting pore geometries is needed.

We showed that temperature responsive HNP membranes are mechanically robust at both room and elevated temperature and proposed that this is the result of polymer-polymer interactions, in which the polymer brushes act as a "molecular glue". Our simulation shed further light on these polymer-polymer interactions, showing the formation of polymer "bridges" that connect neighboring HNPs.

Temperature responsive HNP membranes combine several attractive properties, including simple self-assembly preparation from nanoscale building blocks, tunable nanopore size, control of nanofiltration cut-off and water permeability by temperature, and high flux at low pressure. These membranes can be prepared with thicknesses ranging from a few microns to a few hundred microns and with a large surface area. The observed high permeability of PNIPAM-HNP membranes to water molecules combined with high filtration size selectivity makes them particularly attractive for separations,[62] but also in preparation of responsive microfluidic devices.

Author information

Corresponding Authors
*Email: i.zharov@utah.edu,
michael.gruenwald@utah.edu.
Author Contributions
†These authors contributed equally to this work.
Notes
The authors declare no competing financial interest.

Acknowledgements

This work was supported by the National Science Foundation (grants no. CHE-1710052 and DMR-1848499). The support and resources from the Center for High Performance Computing at the University of Utah are gratefully acknowledged.

Supporting information

Computational methods, model parameterization, pore size calculations, thermogravimetric analysis and water flux data. This material is available free of charge via the Internet at http://pubs.acs.org.

References

1. Scott, K. *Handbook of Industrial Membranes*; 1st ed.; Elsevier Science Publishers LTD: Oxford, 1995.
2. van Reis, R.; Zydney, A. Bioprocess Membrane Technology. *J. Memb. Sci.* **2007**, *297*, 16–50.
3. Wei, L.; Kawamoto, K. Upgrading of Simulated Syngas by Using a Nanoporous Silica Membrane Reactor. *Chem. Eng. Technol.* **2013**, *36*, 650–656.
4. Pendergast, M. M.; Hoek, E. M. V. A Review of Water Treatment Membrane Technology: Processes, Performance, and Future Directions. *Energy Environ. Sci.* **2011**, *4*, 1946–1971.
5. Deng, J.; Toh, C.-S. Impedimetric DNA Biosensor Based on a Nanoporous Alumina Membrane for the Detection of the Specific Oligonucleotide Sequence of Dengue Virus. *Sensors* **2013**, *13*, 7774–7785.
6. Adiga, S. P.; Jin, C.; Curtiss, L. A.; Monteiro-Riviere, N. A.; Narayan, R. J. Nanoporous Membranes for Medical and Biological Applications. *Wiley Interdiscip. Rev. Nanomedicine Nanobiotechnology* **2009**, *1*, 568–581.
7. Schepelina, O.; Poth, N.; Zharov, I. pH-Responsive Nanoporous Silica Colloidal Membranes. *Adv. Funct. Mater.* **2010**, *20*, 1962-1969.
8. Bohaty, A. K.; Newton, M. R.; Zharov, I. Light-Controlled Ion Transport through Spiropyran-Modified Nanoporous Silica Colloidal Films. *J. Porous Mater.* **2010**, *17*, 465-473.
9. Abelow, A. E.; Persson, K.; Berggren, M.; Zharov, I. Electroresponsive Nanoporous Membranes by Coating Anodized Alumina with Poly(3,4-ethylenedioxythiophene) and Polypyrrole. *Macromol. Mater. Eng.* **2014**, *299*, 190-197.
10. Wandera, D.; Wickramasinghe, S. R..; Husson, S. M. Stimuli-Responsive Membranes. *J. Membr. Sci.* **2010**, *357*, 6–35.
11. Ulbricht, M. Advanced Functional Polymer Membranes. *Polymer* **2006**, *47*, 2217–2262.
12. Querelle, S. E.; Jackson, E. A.; Cussler, E. A.; Hillmyer, M. A. Ultrafiltration Membranes with a Thin Poly(Styrene)-B-Poly(Isoprene) Selective Layer. *ACS Appl. Mater. Interfaces*, **2013**, *5*, 5044–5050.
13. Peinemann, K.-V.; Abetz, V.; Simon, P. F. W. Asymmetric Superstructure Formed in a Block Copolymer via Phase Separation. *Nature Mater.* **2007**, *6*, 992–996.
14. Peng Lee, K.; Mattia, D. Monolithic Nanoporous Alumina Membranes for Ultrafiltration Applications: Characterization, Selectivity–Permeability Analysis and Fouling Studies. *J. Membr. Sci.* **2013**, *435*, 52–61.
15. Chang, Y.; Ling, Z.; Liu, Y.; Hu, X.; Li, Y. A Simple Method for Fabrication of Highly Ordered Porous α-Alumina Ceramic Membranes. *J. Mater. Chem.* **2012**, *22*, 7445–7448.
16. Chiang, A. S. T.; Chao, K.-J. Preparation and Characterization of Novel Porous Membranes with Different Surface Morphologies. *J. Phys. Chem. Solids* **2001**, *62*, 1899–1910.
17. Willott, D. J.; Nielen, W. M.; de Vos, W. M. Stimuli-Responsive Membranes through Sustainable Aqueous Phase Separation. *ACS Appl. Polymer Mater.* **2020**, *2*, 659–667.
18. Sadeghi, I.; Kronenberg, J.; Asatekin, A. Selective Transport through Membranes with Charged Nanochannels Formed by Scalable Self-Assembly of Random Copolymer Micelles. *ACS Nano* **2018**, *12*, 95–108.
19. Li, Y.; Chu, L.-Y.; Zhu, J. H.; Wang, H.-D.; Xia, H.-L.; Chen, W.-M. Thermoresponsive Gating Characteristics of Poly(N-isopropylacrylamide)-Grafted Porous Poly(vinylidene fluoride) Membranes. *Ind. Eng. Chem. Res*. **2004**, *43*, 2643–2649.
20. Peng, T.; Cheng, Y.-L. Temperature-Responsive Permeability of Porous PNIPAAm-g-PE Membranes, *J. Appl. Polym. Sci.* **1998**, *70*, 2133-2142.
21. Li, S. K.; D'Emanuele, A. On-Off Transport through a Thermoresponsive Hydrogel Composite Membrane. *J. Contr. Rel.* **2001**, *75*, 55-67.
22. Rama Rao, G. V.; Lopez, G. Encapsulation of Poly(N-Isopropyl Acrylamide) in Silica: A Stimuli-Responsive Porous Hybrid Material That Incorporates Molecular Nano-Valves. *Adv. Mater.* **2000**, 12**,** 1692-1695.
23. Schepelina, O.; Zharov, I. PNIPAAM-Modified Nanoporous Colloidal Films with Positive and Negative Temperature Gating. *Langmuir* **2007**, *23*, 12704–12709.
24. Zharov, I.; Khabibullin, A. Surface-Modified Silica Colloidal Crystals: Nanoporous Films and Membranes with Controlled Ionic and Molecular Transport. *Acc. Chem. Res.* **2014**, *47*, 440–449.
25. Schaep, J.; Van der Bruggen, B.; Vandecasteele, C.; Wilms, D. In *Chemistry for the Protection of the Environment 3*; Springer US: Boston, MA, 1998; pp 117–125.
26. Khabibullin, A.; Fullwood, E.; Kolbay, P.; Zharov, I. Reversible Assembly of Tunable Nanoporous

Materials from "Hairy" Silica Nanoparticles. *ACS Appl. Mater. Interfaces* **2014**, *6*, 17306-17312.
27. Nge, P. N.; Yang, W.; Pagaduan, J. V.; Woolley, A. T. Ion-Permeable Membrane for On-chip Preconcentration and Separation of Cancer Marker Proteins. *Electrophoresis* **2011**, *32*, 1133–1140.
28. Scott, K. *Handbook of Industrial Membranes*, 1st ed.; Elsevier Science Publishers LTD: Oxford, 1995.
29. Eygeris, Y.; White, E. V; Wang, Q.; Carpenter, J. E.; Grünwald, M.; Zharov, I. Responsive Nanoporous Membranes with Size Selectivity and Charge Rejection from Self-Assembly of Polyelectrolyte "Hairy" Nanoparticles. *ACS Appl. Mater. Interfaces* **2019**, *11*, 3407–3416.
30. White, E. M.; Yatvin, J.; Grubbs, J. B.; Bilbrey, J. A.; Locklin, J. Advances in Smart Materials: Stimuli-Responsive Hydrogel Thin Films. *J. Polym. Sci. Part B Polym. Phys.* **2013**, *51*, 1084–1099.
31. Adiga, S. P.; Brenner, D. W. Stimuli-Responsive Polymer Brushes for Flow Control through Nanopores. *J. Funct. Biomater.* **2012**, *3*, 239–256.
32. Zhang, Y.-Y.; He, X.-W.; Li, W.-Y. Study on the Room Temperature Synthesis of Highly Photoluminescent and Temperature-Sensitive CDs/PNIPAM Hybrid Hydrogels and Their Properties. *RSC Adv.* **2015**, *5*, 71030–71034.
33. Pelton, R. Temperature-Sensitive Aqueous Microgels. *Adv. Colloid Interface Sci.* **2000**, *85*, 1–33.
34. Fujishige, S.; Kubota, K.; Ando, I. Phase Transition of Aqueous Solutions of Poly(N-isopropylacrylamide) and Poly(N-isopropylmethacrylamide). *J. Phys. Chem.* **1989**, *93*, 3311–3313.
35. Schmaljohann, D. Thermo- and pH-Responsive Polymers in Drug Delivery. *Adv. Drug Deliv. Rev.* **2006**, *58*, 1655–1670.
36. Luzinov, I.; Minko, S.; Tsukruk, V. V. Responsive Brush Layers: from Tailored Gradients to Reversibly Assembled Nanoparticles. *Soft Matter.* **2008**, *4*, 714–25.
37. Wu, T.; Zhang, Y.; Wang, X.; Liu, S. Fabrication of Hybrid Silica Nanoparticles Densely Grafted with Thermoresponsive Poly(N-isopropylacrylamide) Brushes of Controlled Thickness via Surface-Initiated Atom Transfer Radical Polymerization. *Chem. Mater.* **2008**, *20*, 101–109.
38. Ishida, N.; Biggs, S. Effect of Grafting Density on Phase Transition Behavior for Poly(N-isopropylacryamide) Brushes in Aqueous Solutions Studied by AFM and QCM-D. *Macromolecules* **2010**, *43*, 7269–7276.
39. Lin, G.; Chang, S.; Kuo, C. H.; Magda, J.; Solzbacher, F. Free Swelling and Confined Smart Hydrogels for Applications in Chemomechanical Sensors for Physiological Monitoring. *Sens. Actuators B Chem.* **2009**, *136*, 186–195.
40. Rittigstein, P.; Priestley, R. D.; Broadbelt, L. J.; Torkelson, J. M. Model Polymer Nanocomposites Provide an Understanding of Confinement Effects in Real Nanocomposites. *Nat. Mater.* **2007**, *6*, 278–282.
41. Chevigny, C. E.; Dalmas, F.; Cola, E. Di; Gigmes, D.; Bertin, D.; Bou, F.-O.; Jestin, J. Polymer-Grafted-Nanoparticles Nanocomposites: Dispersion, Grafted Chain Conformation, and Rheological Behavior. *Macromolecules* **2011**, *44*, 122–133.
42. Åkerman, S.; Viinikka, P.; Svarfvar, B.; Putkonen, K.; Järvinen, K.; Kontturi, K.; Näsman, J.; Urtti, A.; Paronen, P. Drug Permeation Through a Temperature-Sensitive Poly(N-Isopropylacrylamide) Grafted Poly(Vinylidene Fluoride) Membrane. *Int. J. Pharm.* **1998**, *164*, 29–36.
43. Khabibullin, A.; Zharov, I. Nanoporous Membranes with Tunable Pore Size by Pressing/Sintering Silica Colloidal Spheres. *ACS Appl. Mater. Interfaces* **2014**, *6*, 7712–7718.
44. Stöber, W.; Fink, A.; Bohn, E. Controlled Growth of Monodisperse Silica Spheres in the Micron Size Range. *J. Colloid Interface Sci.* **1968**, *26*, 62–69.
45. Min, K.; Gao, H.; Matyjaszewski, K. Use of Ascorbic Acid as Reducing Agent for Synthesis of Well-Defined Polymers by ARGET ATRP. *Macromolecules* **2007**, *40*, 1789–1791.
46. Fan, Z.; Grünwald, M. Orientational Order in Self-Assembled Nanocrystal Superlattices. *J. Am. Chem. Soc.* **2019**, *141*, 1980–1988.
47. Léonforte, F.; Müller, M. Poly(N-isopropylacrylamide)-Based Mixed Brushes: A Computer Simulation Study. *ACS Appl. Mat. & Interfaces* **2015**, *7*, 12450–12462.
48. Anderson, J. A.; Glaser, J.; Glotzer, S. C. HOOMD-Blue: A Python Package for High-Performance Molecular Dynamics and Hard Particle Monte Carlo Simulations. *Comp. Mater. Sci.* **2020**, *173*, 109363.
49. Schmitt, M.; Choi, J.; Min Hui, C.; Chen, B.; Korkmaz, E.; Yan, J.; Margel, S.; Burak Ozdoganlar, O.; Matyjaszewski, K.; Bockstaller, M. R. Processing Fragile Matter: Effect of Polymer Graft Modification on the Mechanical Properties and Processibility of (Nano-) Particulate Solids. *Soft Matter* **2016**, *12*, 3527–3537.

50. Carman, P. C. Fluid Flow through Granular Beds. *Chem. Eng. Res. Des.* **1997**, *75*, S32–S48.
51. Ozgumus, T.; Mobedi, M.; Ozkol, U. Determination of Kozeny Constant Based on Porosity and Pore to Throat Size Ratio in Porous Medium with Rectangular Rods. *Eng. Appl. Comput. Fluid Mech.* **2014**, *8*, 308–318.
52. Kilgour, D. M.; Scott, G. D. The Density of Random Close Packing of Spheres. *J. Phys. D. Appl. Phys.* **1969**, *2*, 863–866.
53. Gilbert, E. P.; Nelson, A.; Prescott, S. W.; Webber, G. B.; Wanless, E. J.; Murdoch, T. J.; Humphreys, B. A. Influence of Molecular Weight on PNIPAM Brush Modified Colloidal Silica Particles. *Soft Matter* **2018**, *15*, 55–64.
54. Bittrich, E.; Burkert, S.; Müller, M.; Eichhorn, K. J.; Stamm, M.; Uhlmann, P. Temperature-Sensitive Swelling of Poly(N-isopropylacrylamide) Brushes with Low Molecular Weight and Grafting Density. *Langmuir* **2012**, *28*, 3439–3448.
55. Ignacio-de Leon, P. A. A.; Eygeris, Y.; Haynes, R.; Zharov, I. Diffusion of Proteins across Silica Colloidal Crystals. *Langmuir* **2018**, *34*, 10333–10339.
56. Smith, J. J.; Zharov, I. Ion Transport in Sulfonated Nanoporous Colloidal Films. *Langmuir* **2008**, *24*, 2650–2654.
57. Ignacio-de Leon, P. A.; Zharov, I. Size-Selective Molecular Transport through Silica Colloidal nNanopores. *Chem. Commun.* **2011**, *47*, 553–555.
58. Bohaty, A. K.; Smith, J. J.; Zharov, I. Free-Standing Silica Colloidal Nanoporous Membranes. *Langmuir* **2009**, *25*, 3096–3101.
59. De Gennes, P. G. Scaling Theory of Polymer Adsorption. *J. de Physique* **1976**, *37*, 1445–1452.
60. Waltmann, C.; Horst, N.; Travesset, A. Capping Ligand Vortices as “Atomic Orbitals” in Nanocrystal Self-Assembly. *ACS Nano* **2017**, *11*, 11273–11282.
61. Fan. Z.; Gruenwald, M. Energy vs. Entropy in Superlattices of Ligand-Covered Nanoparticles. ChemRxiv. Cambridge: Cambridge Open Engage; 2019.
62. Park, H. B.; Kamcev, J.; Robeson, L. M.; Elimelech, M.; Freeman, B. D. Maximizing The Right Stuff: The Trade-Off Between Membrane Permeability And Selectivity. *Science* **2017**, *356*, 1138–1148.

Table of Contents Graphic